*Pramana – J. Phys.* (2019) 93:20
https://doi.org/10.1007/s12043-019-1770-y


# The effect of thermal expansion coefficient on unsteady non-Newtonian supercritical Casson fluid flow past a vertical cylinder

ASHWINI HIREMATH[1], HUSSAIN BASHA[1], BHASKERREDDY KETHIREDDY[1], G JANARDHANA REDDY[1,*] and N S VENKATA NARAYANAN[2]

[1]Department of Mathematics, Central University of Karnataka, Kalaburagi 585 367, India
[2]Department of Chemistry, Central University of Karnataka, Kalaburagi 585 367, India
*Corresponding author. E-mail: gjr@cuk.ac.in

MS received 17 June 2018; revised 6 December 2018; accepted 27 December 2018; published online 21 May 2019

**Abstract.** A new thermodynamic computational model has been proposed for the current study, which deals with the free convective supercritical Casson fluid flow past a vertical cylinder. In this model, pressure, temperature and compressibility factor are the critical parameters to govern the thermal expansion coefficient. The present model is based on the Redlich–Kwong equation of state. Comparisons with experimental results and determined values of thermal expansion coefficient for the choice of chemical compound (isobutene) from the present study show great similarity. The chemical compound isobutane has many industrial applications. For instance, in geothermal power plant, supercritical isobutane is employed as a working fluid, it is used in the deactivated (USY alkylation) catalyst regeneration, it is used in heat pumps and many other industrial processes. Furthermore, isobutane finds extensive application as a propellant in foam products and aerosol cans, as a refrigerate gas in freezers and refrigerators, as a feedstock in industries of petrochemical importance, for standardisation of gas mixtures and emission monitoring, etc. In addition, the Casson fluid flow model can be used to study the blood flow rheology, slurry flows, etc. The numerical scheme such as Crank–Nicolson type is demonstrated to simplify the governing nonlinear coupled partial differential equations. The transient results of flow-field variables, coefficients of heat and momentum transport for a Casson fluid under supercritical condition for various values of reduced pressure and reduced temperature are computed and discussed through graphs.

**Keywords.** Thermal expansion coefficient; supercritical Casson fluid; isobutane ($C_4H_{10}$); vertical cylinder; reduced temperature; reduced pressure.

**PACS Nos 05.70.Ce; 05.70.Fh; 44.25.+f; 47.00**

## 1. Introduction

Any substance or a compound at specific conditions of temperature and pressure above its critical point can be described by its incapability to differentiate whether it is present in a gaseous state or a liquid state. The fluids that exhibit such intermediate behaviour are termed as supercritical fluids (SCF). The supercritical phenomenon at high pressure and temperature is a trending area of study since decades because of its vital importance in polymers, powders, natural products, cosmetics, biotechnology, pharmaceuticals, biofuels, fossils, etc. In addition, the processes such as purification, polymerisation, crystallisation, extraction, atomisation, separation, drying, solubilisation, cleaning and many more are characterised by the SCF phenomenon. Baron Charles Cagniard de la Tour discovered SCF for the first time in 18th century by conducting experiments on cannon balls.

Recently, investigation of heat transfer problems with particular importance to free convection has become the emerging area of research. In the beginning, Sparrow and Gregg [1] have worked out the problem of a heated vertical cylinder. Further, Lee *et al* [2] considered the problem of a similar type for the same flow geometry with power-law variation. However, the research in heat transfer for free convection under SCF region is still very

much essential. Some remarkable studies on SCF are mentioned in [3–17].

Isobutane, also known by its chemical name methylpropane, is an odourless and colourless gas. It is the simplest alkane with a tertiary carbon of molecular formula $C_4H_{10}$. This is an isomer of butane and it is used as a replacement for chlorofluorocarbon (CFC) in many applications such as cleansing products, deodorant, shaving cream, propellant for hairspray, petrol additive, portable camp stove, and as an aerosol. Isobutane is chosen for the current study in SCF region because of its outstanding properties, for instance, it has smaller ozone layer depletion potentials, it has minimal effect in global warming and it has low critical pressure. Further, it is used in geothermal power generation, as a refrigerant, etc. [18–27].

Most of the studies on SCF were confined to Newtonian fluid only. The limitations of the classical fluid theory have encouraged the scope for non-Newtonian fluid. The choice of non-Newtonian fluid for the present study is Casson fluid. It is obviously important because of its critical usage in daily life. It has well-defined rheological properties compared to other viscoplastic fluid models. This particular fluid belongs to the category of shear thinning liquid with the assumption of 'having an infinite viscosity at zero rate of shear, a yield stress below which no flow occurs and zero viscosity at an infinite rate of shear [28]'. Hand cream, honey, blood, gelatin, jelly, milk, ink, etc. are some of the examples belonging to the class of Casson fluid. Some of the research contributions on Casson fluid are listed in [29–31]. Very recently, Janardhana Reddy *et al* [32,33] have worked out the problems on cylinder geometry with Casson fluid. They also studied the heatline visualisation [32] and entropy generation [33].

The aim of the present work is to study the transient boundary layer flow characteristics of 'supercritical Casson fluid of isobutane over an isothermal vertical cylinder'. The current investigation is very significant due to the versatile usage of isobutane. The present model considers the equation of state (EOS) for predicting the supercritical flow characteristics of Casson fluid in terms of isobutane. For the first time, an attempt has been made through this research paper 'to study the buoyancy-driven boundary layer region around an isothermal vertical cylinder which is kept in supercritical Casson fluid'. A 'finite difference implicit scheme of Crank–Nicolson type' is used as the computational tool. Numerically simulated values are recorded for the selected compound isobutane. The influence of isobutane in 'supercritical' region pertaining to the Casson fluid flow variables, heat and momentum transport coefficients are observed significantly and corroborated with those of the existing theoretical or reference results.

## 2. Equation for $\beta$ in supercritical Casson fluid region based on Redlich–Kwong equation of state (RK-EOS)

In most of the studies (free-convective flow under the Boussinesq approximation), it is assumed that the volumetric coefficient of thermal expansion ($\beta$) is a constant. Similarly, the variation of $\beta$ with respect to 'pressure and temperature' is omitted. However, under SCF region, the results obtained can be erroneous with this assumption. Hence, to evaluate $\beta$, a suitable equation of state is required. In this paper, RK-EOS [34] is used to calculate $\beta$ in terms of compressibility factor ($Z$), temperature ($T'$) and pressure ($P$).

The thermodynamic equation to calculate $\beta$ based on RK-EOS is given by [16,34]

$$\beta = \frac{1}{T'}\left[1 - \left(\frac{3.5AB + 2ZB^2 + BZ - 2.5AZ}{3Z^3 - 2Z^2 + Z(A-B) - B^2Z}\right)\right], \tag{1}$$

where

$$Z = \frac{PV'}{R'T'}, \quad A = \frac{aP}{\sqrt{T'}(R'T')^2}, \quad B = \frac{bP}{R'T'}.$$

Similarly, the expression for $\beta$ using VW-EOS [35] is given by

$$\beta = \frac{1}{T'}\left[1 - \left(\frac{2Z^2B - 2ZA + 3AB}{3Z^3 - 2Z^2(B+1) - AZ}\right)\right], \tag{2}$$

where

$$Z = \frac{PV'}{R'T'}, \quad A = \frac{aP}{(R'T')^2}, \quad B = \frac{bP}{R'T'}.$$

Furthermore, the reduced temperature and reduced pressure are defined as $T_r^* = T'/T_c$ and $P_r^* = P/P_c$. In eqs (1) and (2), $T'$ is the temperature, $P$ is the pressure, $Z$ is the compressibility factor, $V'$ is the molar volume, $R'$ is the universal gas constant, $A$ and $B$ are the RK-EOS constants, $T_c$ is the critical temperature, $P_c$ is the critical pressure and further, figure 1a shows the phase diagram of isobutane.

## 3. Formulation of the research problem

For supercritical Casson fluid, the transient free-convective flow over a vertical cylinder in a two-dimensional region is deliberated, and the respective flow geometry is reflected in figure 1b. The $x$- and $r$-coordinates are assumed along the axis of the cylinder (vertically upward) and normal to the cylinder, respectively. The governing equations are defined by neglecting the effect of viscous dissipation. In addition,

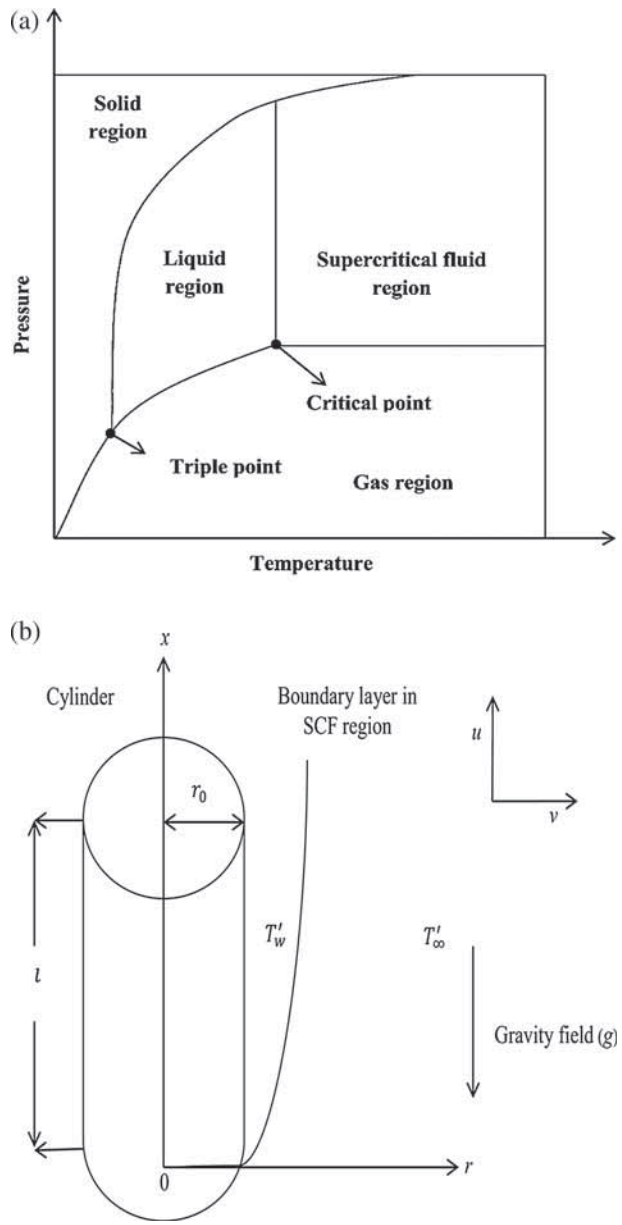


**Figure 1.** (**a**) Phase diagram and (**b**) physical model of the current problem.

the rheological equation for a viscous incompressible Casson fluid flow is given by [36,37]

$$\tau_{ij} = \begin{cases} \left(2\mu_{\mathrm{B}} + \sqrt{2}p_y/\sqrt{\pi}\right)e_{ij}, & \pi > \pi_{\mathrm{c}}, \\ \left(2\mu_{\mathrm{B}} + \sqrt{2}p_y/\sqrt{\pi_{\mathrm{c}}}\right)e_{ij}, & \pi < \pi_{\mathrm{c}}. \end{cases} \tag{3}$$

The symbols involved in the tensor ($\tau_{ij}$) are explained in detail in the available literature [33]. Considering the abovementioned assumptions and Boussinesq approximation for SCF, the governing equations have been formulated as eqs (4)–(6) for supercritical Casson fluid flow across the boundary layer region [28–34]:

$$\frac{\partial(ru)}{\partial x} + \frac{\partial(rv)}{\partial r} = 0, \tag{4}$$

$$\rho\left(\frac{\partial u}{\partial t'} + u\frac{\partial u}{\partial x} + v\frac{\partial u}{\partial r}\right) = \rho g\beta(T' - T'_\infty) + \mu\left(1 + \frac{1}{\beta_{\mathrm{c}}}\right)\left(\frac{\partial^2 u}{\partial r^2} + \frac{1}{r}\frac{\partial u}{\partial r}\right), \tag{5}$$

$$u\frac{\partial T'}{\partial x} + v\frac{\partial T'}{\partial r} + \frac{\partial T'}{\partial t'} = \frac{\alpha}{r}\frac{\partial}{\partial r}\left(r\frac{\partial T'}{\partial r}\right), \tag{6}$$

where $\beta_{\mathrm{c}} = \mu_{\mathrm{B}}\sqrt{2\pi_{\mathrm{c}}}/p_y$ is the Casson fluid parameter.

The initial ($t' \leq 0$) and boundary ($t' > 0$) conditions to solve eqs (4)–(6) are given below:

$$\left.\begin{array}{l} t' \leq 0 : u = 0;\ T' = T'_\infty;\ v = 0\,\forall\, x \text{ and } r \\ t' > 0 : u = 0;\ T' = T'_{\mathrm{w}};\ v = 0 \text{ at } r = r_0 \\ u = 0;\ T' = T'_\infty;\ v = 0 \text{ at } x = 0 \\ u \to 0;\ T' \to T'_\infty;\ v \to 0 \text{ as } r \to \infty \end{array}\right\}. \tag{7}$$

In eqs (4)–(7), $u$, $v$ are the components of velocity along $x$ and $r$ coordinates, $t'$ is the dimensional time, $\rho$ is the fluid density, $g$ is the acceleration due to gravity, thermal expansion coefficient is denoted with $\beta$, dynamic viscosity is indicated with $\mu$, $P_y$ is the yield stress, $\alpha$ is the thermal diffusivity, $r_0$ is the radius of the cylinder, free stream temperature is denoted by $T'_\infty$ and $T'_{\mathrm{w}}$ is the wall temperature.

However, the present physical problem involves the system of nonlinear coupled partial differential equations (4)–(6), with appropriate conditions (7), is difficult to solve directly in the dimensional form. Therefore, to avoid this difficulty, we have used non-dimensionalisation process, which reduces the dimensional governing equations to their non-dimensional forms. It is clear that non-dimensionalisation is a technique of removing the units from the equation of a physical problem in partial or full scale by substituting appropriate parameters (variables). This practice can abridge and parameterise problems where the measured units are involved. In particular, the dimensionless approach typically generalises the problem. In view of these reasons, the following dimensionless physical quantities are used.

Consider the below non-dimensional numbers and substitute:

$$\left.\begin{array}{l} X = \mathrm{Gr}^{-11/12}\dfrac{x}{r_0}, \quad R = \dfrac{r}{r_0}, \quad U = \mathrm{Gr}^{-11/12}\dfrac{ur_0}{\vartheta} \\ V = \dfrac{vr_0}{\vartheta}, \quad t = \dfrac{\vartheta t'}{r_0^2}, \quad \theta = \dfrac{T' - T'_\infty}{T'_{\mathrm{w}} - T'_\infty} \\ \mathrm{Gr} = \dfrac{g\beta r_0^3\left(T'_{\mathrm{w}} - T'_\infty\right)}{\vartheta^2}, \quad \mathrm{Pr} = \dfrac{\vartheta}{\alpha} \end{array}\right\}. \tag{8}$$

In eqs (4)–(7), they are abridged to the following form:

$$\frac{\partial U}{\partial X}+\frac{\partial V}{\partial R}+\frac{V}{R}=0, \tag{9}$$

$$\frac{\partial U}{\partial t}+U\frac{\partial U}{\partial X}+V\frac{\partial U}{\partial R}=\mathrm{Gr}^{1/12}\theta + \left(1+\frac{1}{\beta_c}\right)\left(\frac{\partial^2 U}{\partial R^2}+\frac{1}{R}\frac{\partial U}{\partial R}\right), \tag{10}$$

$$\frac{\partial \theta}{\partial t}+U\frac{\partial \theta}{\partial X}+V\frac{\partial \theta}{\partial R}=\frac{1}{\mathrm{Pr}}\left(\frac{\partial^2 \theta}{\partial R^2}+\frac{1}{R}\frac{\partial \theta}{\partial R}\right). \tag{11}$$

The conditions at initial time ($t \leq 0$) and boundary ($t > 0$) in non-dimensional form are given below:

$$\left.\begin{array}{l} t \leq 0 : \theta = 0, \quad U = 0, \quad V = 0 \quad \forall\, X \text{ and } R \\ t > 0 : \theta = 1, \quad U = 0, \quad V = 0 \quad \text{at } R = 1 \\ \theta = 0, \quad U = 0, \quad V = 0 \quad \text{at } X = 0 \\ \theta \to 0, \quad U \to 0, \quad V \to 0 \quad \text{as } R \to \infty \end{array}\right\}. \tag{12}$$

In eqs (8)–(12), $U$ and $V$ are the components of non-dimensional velocity along $X$ and $R$ directions, $\vartheta$ is the kinematic viscosity, Gr is the Grashof number, Pr is the Prandtl number, $\theta$ is the non-dimensional temperature and $t$ is the dimensionless time.

The physical significance of non-dimensional parameters used in this study is as follows:

(i) $\beta_c$ can be used to determine the viscoplastic (pseudoplastic) behaviour of Casson fluid;
(ii) Gr signifies the buoyancy-induced natural convection flow;
(iii) Pr gives the relative thickness of 'thermal boundary layer to the momentum boundary layer'.

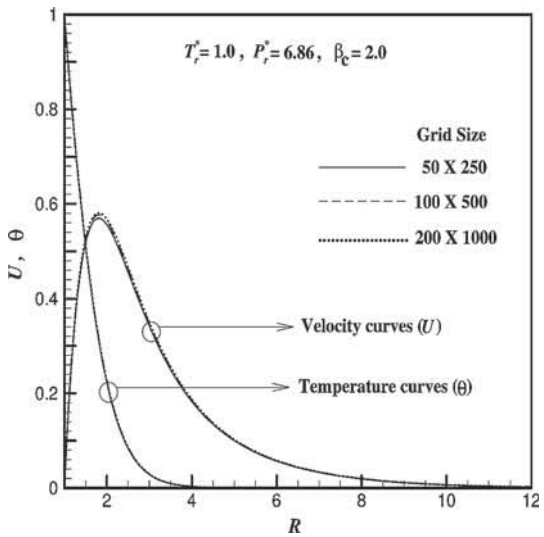


**Figure 2.** Grid independency test for the selection of grid size in the supercritical Casson fluid region.

## 4. Solution methodology using a finite difference scheme

The set of unsteady nonlinear-coupled partial differential equations along with conditions (non-dimensional), i.e. eqs (9)–(12), which describe the supercritical Casson fluid flow past a vertical cylinder, is sufficiently complex. The failure of analytical methods for the simplification of this set of complicated equations suggests a numerical method to get an approximate solution. Here, a compatible implicit iterative method with characteristics of unconditionally stable and fast convergence is used, which is explained in [38]. The solution domain varies from $X_{\min} = 0$ to $X_{\max} = 1$ and from $R_{\min} = 1$ to $R_{\max}$(or $R = \infty$) $= 20$. A grid independency test ensures the consistency and an economical convenience (refer figure 2) for the selection of mesh size. The criterion of convergence is fixed (as $10^{-5}$) for all flow-field variables.

## 5. Results and discussion

### 5.1 *Validation of RK-EOS model*

The $\beta$ curves with respect to temperature for isobutane at two different pressure conditions based on experimental data [40], perfect gas equation [39], RK-EOS [34] and VW-EOS [35] are shown in figures 3 and 4.

It is evident from figures 3 and 4 that the $\beta$ values calculated based on the RK-EOS have given accurate results and are more comparable with reference data [40] than the values calculated based on VW-EOS. Therefore, the RK-EOS model is the better choice than the VW-EOS and a perfect-gas hypothesis (constant $\beta$). Table 1 provides critical values of isobutane such as $T_c$ (critical temperature), $M$ (molar mass), $P_c$ (critical pressure), $V_c$ (critical volume), $Z_c$ (critical compressibility factor) and $D_c$ (critical density). Table 1 helps in calculating $\beta$ based on the 'thermodynamic models (RK-EOS and VW-EOS) and reference data that are presented in tables 2–4, respectively'. The observations from these tabulations give a clear idea that $\beta$ values calculated from RK-EOS are in better agreement with the experimental data than that of VW-EOS.

The value of $\mathrm{Nu}_X$ as a function of $\mathrm{Ra}_X$ for the 'supercritical isobutane', which is revealed in figure 5 using the 'empirical correlation' equation taken from [41], is of the following form:

$$\frac{\mathrm{Nu}_X}{\mathrm{Ra}_X^{1/4}}=\frac{4}{3}\left\{\frac{7\mathrm{Pr}}{5(20+21\mathrm{Pr})}\right\}^{1/4} + \frac{4(272+315\mathrm{Pr})}{35(64+63\mathrm{Pr})}\left\{\frac{d}{l}\mathrm{Ra}_X^{1/4}\right\}^{-1}. \tag{13}$$

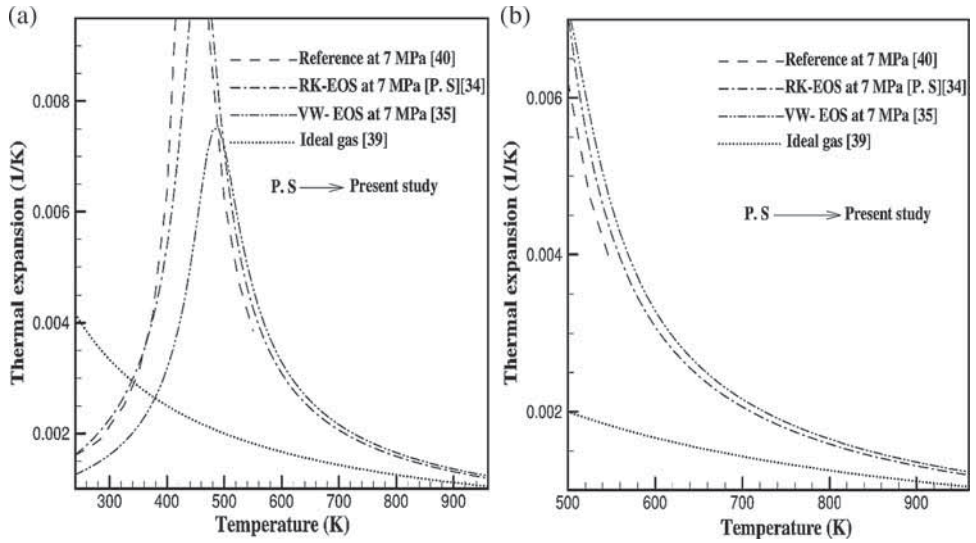


**Figure 3.** (**a**) Comparison of volumetric coefficient of thermal expansion ($\beta$) of isobutane based on VW-EOS [35], perfect-gas assumption [39] and RK-EOS [34] with reference values [40] at 7 MPa and (**b**) an identical graph in the temperature range between 500 and 960 K.

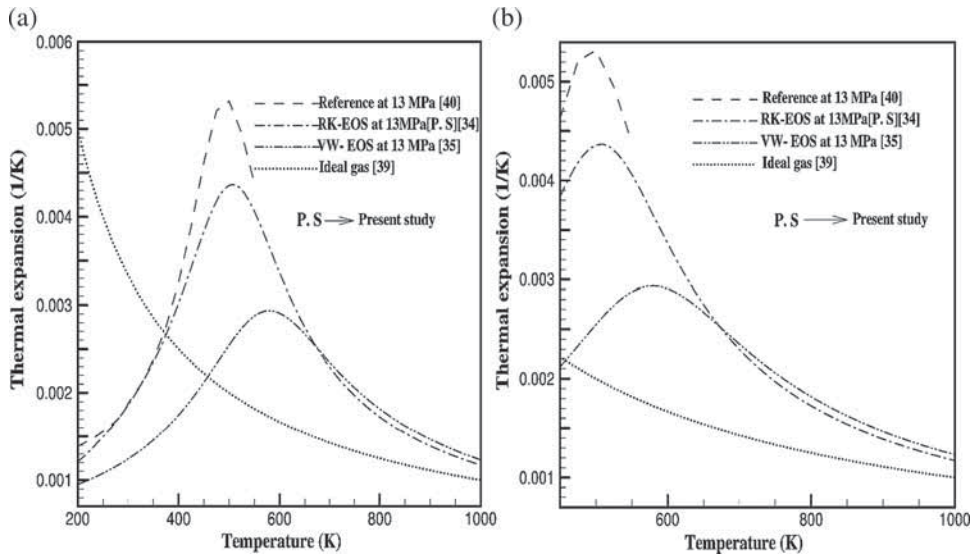


**Figure 4.** (**a**) Comparison of volumetric coefficient of thermal expansion ($\beta$) of isobutane based on VW-EOS [35], perfect-gas assumption [39] and RK-EOS [34] with reference values [40] at 13 MPa and (**b**) an identical graph in the temperature range between 525 and 1000 K.

**Table 1.** Critical values of isobutane [16,40] for calculating the parameters of the fluid.

| Chemical compound | $P_c$ (MPa) | $T_c$ (K) | $V_c$ (cm$^3$/mol) | $M$ (kg/mol) | $D_c$ (kg/m$^3$) | $Z_c$ (−) |
|---|---|---|---|---|---|---|
| Isobutane | 3.640 | 407.85 | 259 | 0.05812 | 224.36 | 0.278 |

**Table 2.** The coefficient of thermal expansion ($\beta$) in the region of SCF based on RK-EOS [34] for various values of pressure ($P$) and temperature ($T'$).

| $P$ (MPa) | $P_r^*$ | $T'$ (K) | $T_r^*$ | $A$ | $B$ | $Z$ | $\beta$ (1/K) |
|---|---|---|---|---|---|---|---|
| 7 | 1.92 | 410 | 1.00 | 0.811342 | 0.165703 | 0.341952 | 0.00613239 |
| 13 | 3.57 | 440 | 1.07 | 1.262924 | 0.286752 | 0.559331 | 0.00367354 |

**Table 3.** The coefficient of thermal expansion ($\beta$) in the region of SCF based on VW-EOS [35] for various values of pressure ($P$) and temperature ($T'$).

| $P$ (MPa) | $P_r^*$ | $T'$ (K) | $T_r^*$ | $A$ | $B$ | $Z$ | $\beta$ (1/K) |
|---|---|---|---|---|---|---|---|
| 7 | 1.92 | 410 | 1.00 | 0.802811 | 0.239124 | 0.417540 | 0.00349887 |
| 13 | 3.57 | 440 | 1.07 | 1.294557 | 0.413808 | 0.672994 | 0.00203842 |

**Table 4.** The coefficient of thermal expansion ($\beta$) in the region of SCF based on reference data [40] for various values of pressure ($P$) and temperature ($T'$).

| $P$ (MPa) | $P_r^*$ | $T'$ (K) | $T_r^*$ | $Z$ | $\beta$ (1/K) |
|---|---|---|---|---|---|
| 7 | 1.92 | 410 | 1.00 | 0.30270 | 0.00673473 |
| 13 | 3.57 | 440 | 1.07 | 0.52272 | 0.00415407 |

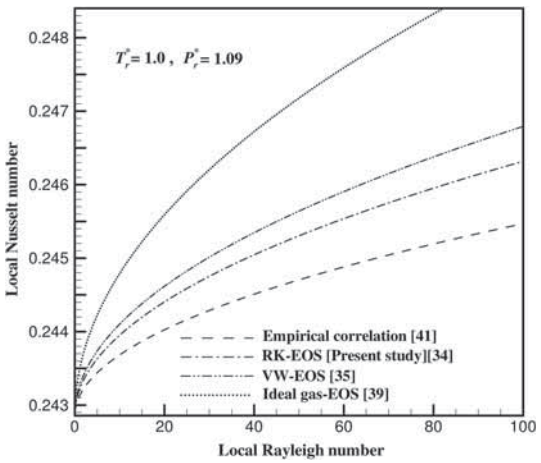


**Figure 5.** Local Nusselt number ($\mathrm{Nu}_X$) as a function of local Rayleigh number ($\mathrm{Ra}_X$) for isobutane when $P_r^* = 1.09$ and $T_r^* = 1.0$ based on VW-EOS [35], RK-EOS [34], experimental correlation [40] and ideal gas-EOS [39].

In eq. (13), $\mathrm{Nu}_X$ is the local Nusselt number, $\mathrm{Ra}_X$ is the local Rayleigh number, $d$ denotes the diameter of the cylinder and $l$ indicates the height of the cylinder. Figure 5 gives the evidence that 'the RK-EOS curve' for $\mathrm{Nu}_X$ against $\mathrm{Ra}_X$ is almost overlapping with empirical correlation curve as than the the ideal gas assumption and VW-EOS curves. This remark ensures that the 'accuracy of RK-EOS model' is more appropriate than the other models for obtaining $\beta$ values and natural convection phenomenon in the SCF region.

### 5.2 *Flow variables*

The flow characteristics are defined for supercritical Casson fluid at different locations under both steady and unsteady states and are shown graphically. The validation of the present problem has been done by comparing

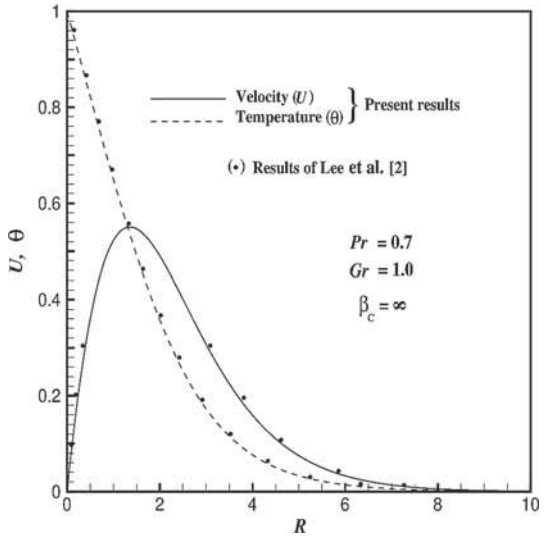


**Figure 6.** Comparison graph for flow variables.

the computational data ($U$ and $\theta$) of the current work for a Newtonian case, i.e. $\beta_c = \infty$ with the results of Lee *et al* [2] for Gr = 1.0 and Pr = 0.7. The simulated data are in good agreement with the earlier results and the same is reflected in figure 6.

At supercritical condition, the simulations are carried out numerically for the selected compound isobutane by taking various values of reduced pressure ($P_r^*$), reduced temperature ($T_r^*$) and Casson fluid parameter ($\beta_c$).

The unsteady $U$ profile at locations (1, 1.4) and (1, 4.0) for different values of $P_r^*$, $T_r^*$ and $\beta_c$ are displayed graphically in figures 7 and 8 vs. time ($t$), respectively. Figures 7 and 8 show the results for velocity at near and far distance from the hot cylindrical wall, respectively. At all locations, the velocity augments with time till the temporal peak is achieved, then the marginal drop occurs subsequently, and in the end, it attains steady state. In the supercritical Casson fluid region, i.e. for all values of $T_r^*$, $P_r^*$ and $\beta_c$, the transient wall velocity curve accelerates monotonically to reach temporal maxima and finally reaches the time-independent state. Initially it is observed that, the conduction governs the heat transfer. After some time, the heat transfer rate is influenced by the effect of the free-convective flow of the supercritical Casson fluid, resulting in increased velocity against time. It can be noticed from figure 7 that for

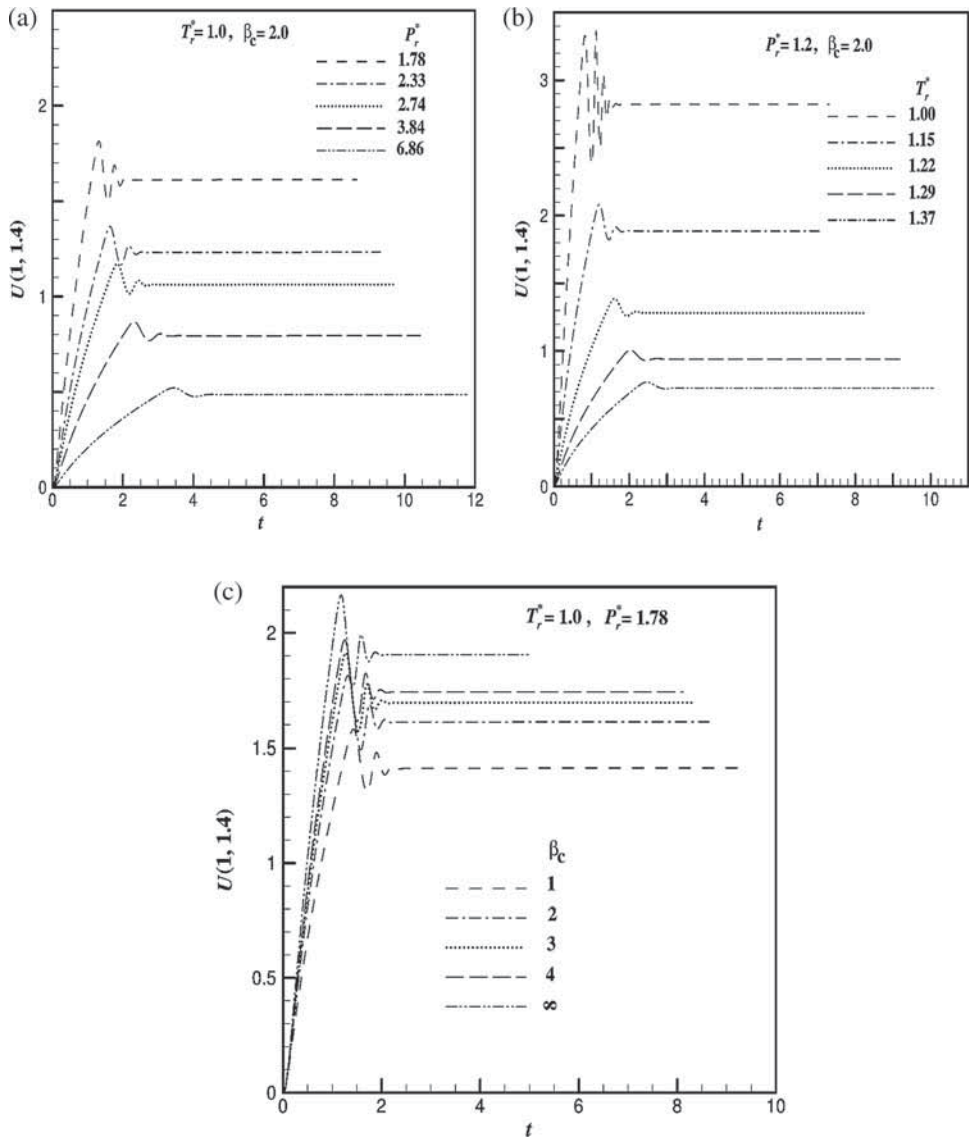


**Figure 7.** Numerically simulated velocity profile ($U$) at (1, 1.4) against time ($t$) for different values of (**a**) $P_r^*$, (**b**) $T_r^*$ and (**c**) $\beta_c$.

increased values of $P_r^*$ or $T_r^*$, the size of the overshoot of the $U$ curves decreases, and the incentive behind this decrement is the decreased velocity diffusion term (refer eq. (10)). Hence, there is a large resistance to the flow of supercritical Casson fluid in the precinct of the temporal peak of $U$. Reverse analysis can be made from figure 7c for increasing values of $\beta_c$. Figures 7a–7c demonstrate the effects of $P_r^*$, $T_r^*$ and $\beta_c$, respectively. Similarly, figure 8 displays the results at a different location. Figures 7a and 7b show that the unsteady velocity field decreases for the increasing $T_r^*$ and $P_r^*$ values. Further, figure 7c illustrates that the transient velocity profile enhances for the increasing values of $\beta_c$. Furthermore, exactly reverse behaviour is noticed in figure 8. Also, from figures 7a–7c, the time needed for attaining the temporal peak value of velocity increases for increasing values of $P_r^*$ and $T_r^*$ and it increases for the decreased values of $\beta_c$. Exactly similar tendency can be found in figure 8. The temperature distribution against time is shown graphically in figure 10 and analysed in later discussion.

Figure 9 represents the $U$ profile in supercritical Casson fluid region against $R$ at $X = 1.0$ for different values of $P_r^*$, $T_r^*$ and $\beta_c$. Figures 9a–9c interpret the effects of different values of $P_r^*$, $T_r^*$ and $\beta_c$, respectively, on velocity profile under steady conditions. In all the three graphs, the $U$ curves begin with zero value close to a cylindrical surface, achieve peak value and again drop to zero value monotonically [for all time ($t$)] in the direction of radial coordinate $R$. The steady-state time augments for the increased values of $T_r^*$ or $P_r^*$. Also, it rises for reduced values of $\beta_c$. The impact of diffusion

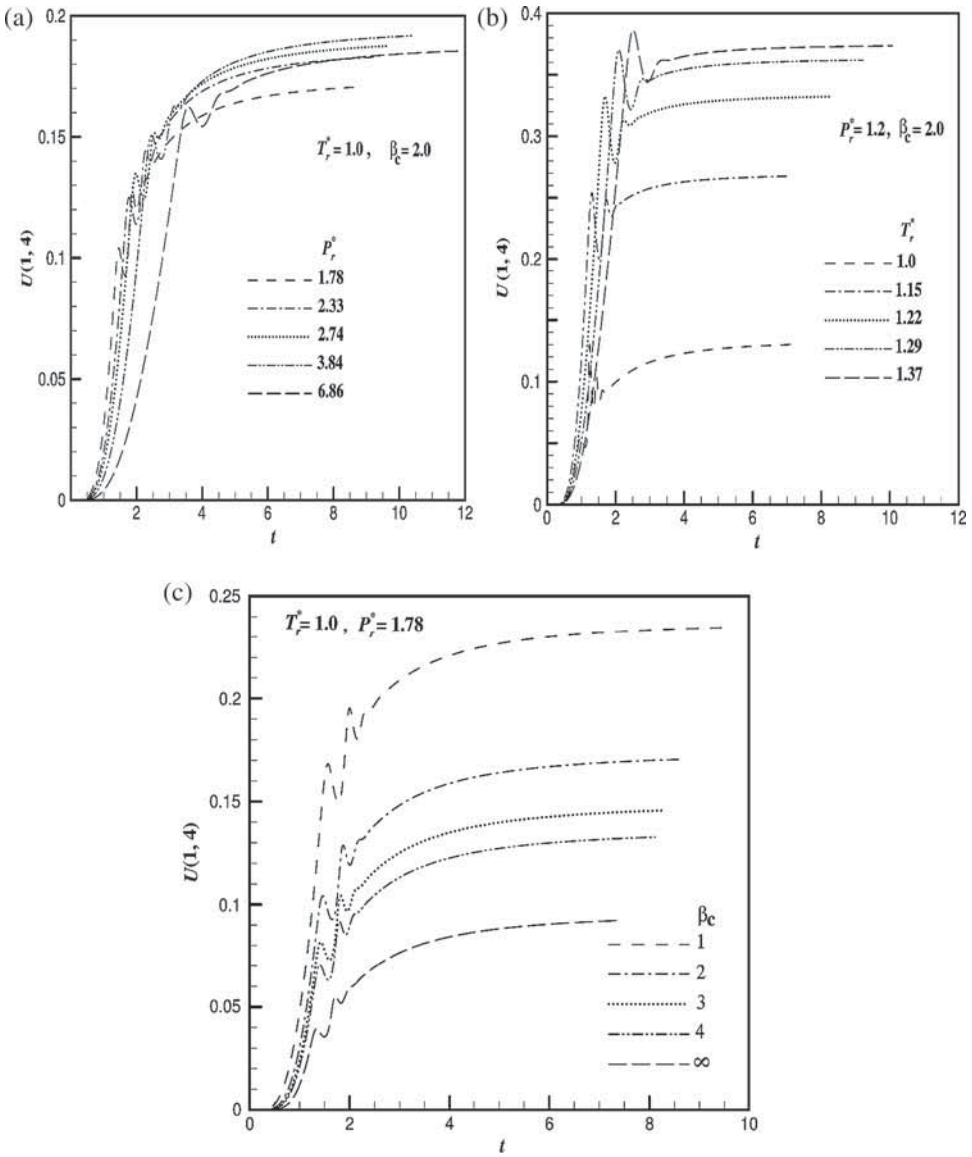


**Figure 8.** Numerically simulated velocity profile ($U$) at (1, 4) against time ($t$) for different values of (**a**) $P_r^*$, (**b**) $T_r^*$ and (**c**) $\beta_c$.

of velocity gets intensified for greater values of $T_r^*$ or $P_r^*$, and thus, diminished velocity curves are noticed, but the reverse trend is noted for Casson fluid parameter (refer figure 9c). When $P_r^*$ and $T_r^*$ increase, the thermal energy convection is confined to the neighbourhood of a heated cylindrical wall, but the momentum diffusion is conveyed far away from the hot cylindrical surface because larger $U$ profiles are observed near the heated wall. From figure 9a, for all values of $P_r^*$ in the supercritical Casson fluid region, i.e. $1 < R < 3.6$, the peak velocity decreases and for $R > 3.6$, the velocity increases. Also, from figure 9b, for all values of $T_r^*$ in the supercritical Casson fluid regions, i.e. $1 < R < 3.20$ and $R > 3.20$, the velocity curves decrease and increase, respectively. Similarly, from figure 9c for all values of $\beta_c$ in the supercritical Casson fluid region, i.e. $1 < R < 2.1$, the peak velocity ($U_{max}$) diminishes and the reverse trend is noticed for $R > 2.1$. The observations from steady flow graphs are well agreed with figures 7 and 8. The steady-state velocity of the supercritical Casson fluid decreases with increasing values of reduced pressure and reduced temperature, but it increases with increasing values of Casson fluid parameter ($\beta_c$). Due to the variation in the velocity field near the boundaries, the cross-flow behaviour is noticed, which is also clearly observed in figures 9a–9c.

In the region of supercritical Casson fluid at (1, 1.45), the $\theta$ profile under an unsteady condition for several values of $P_r^*$ and $T_r^*$ against time ($t$) is displayed in figure 10. The influences of reduced pressure ($P_r^*$),

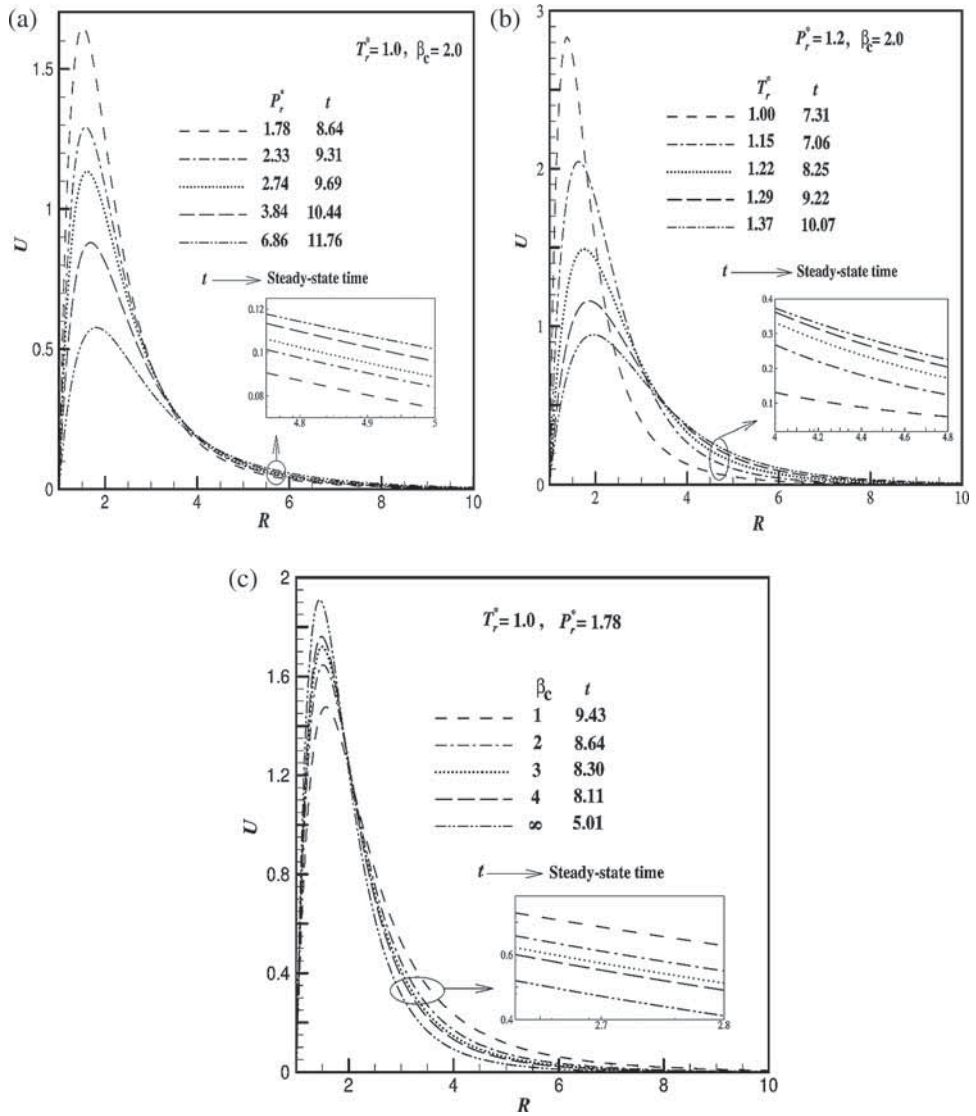


**Figure 9.** Time-independent state velocity profile ($U$) against $R$ when $X = 1.0$ for different values of (**a**) $P_r^*$, (**b**) $T_r^*$ and (**c**) $\beta_c$.

reduced temperature ($T_r^*$) and Casson fluid parameter ($\beta_c$) are shown in figures 10a–10c, respectively. Here, at an initial time, the $\theta$ profiles accelerate with time till the temporal peak is achieved, then decrease, again rises, and at last attains the steady state. These transient effects of the temperature are perceived at other locations ($X$, $R$) also. It is remarked that for increasing $P_r^*$ or $T_r^*$ and decreasing $\beta_c$, the temporal peak time rises. In the beginning, the $\theta$ profile for fixed $P_r^*$ and for variable $T_r^*$ is mainly observed in figure 10b. At the initial phase of time, it is witnessed that the temperature curves are overlapping with each other, and after that, they deviate from one another. Figures 10a and 10c also show the same behaviour for all values of $P_r^*$ and $\beta_c$, respectively. From figure 10b, it is clearly noticed that for $T_r^* = 1.0$, the temperature curve shows a different behaviour due to the existence of a critical point. At starting time, i.e. at the transition from the subcritical to the supercritical region, this curve shows some kind of fluctuations, but these fluctuations are smaller in magnitude and are shown in figure 10a. It is also remarked that near the hot surface, the time-dependent temperature increases for increasing values of $P_r^*$ or $T_r^*$ (refer figures 10a and 10b), and it increases for decreasing values of $\beta_c$ (refer figure 10c).

Figures 11a–11c demonstrate the computer-generated values for $\theta$ profiles at $X = 1.0$ (along $R$) under steady condition for different values of $P_r^*$, $T_r^*$ and $\beta_c$, respectively. These graphical results show that the $\theta$ profiles commence at a hot wall with temperature boundary condition ($\theta = 1$) and monotonically falls along $R$ till the free stream temperature ($\theta = 0$) is

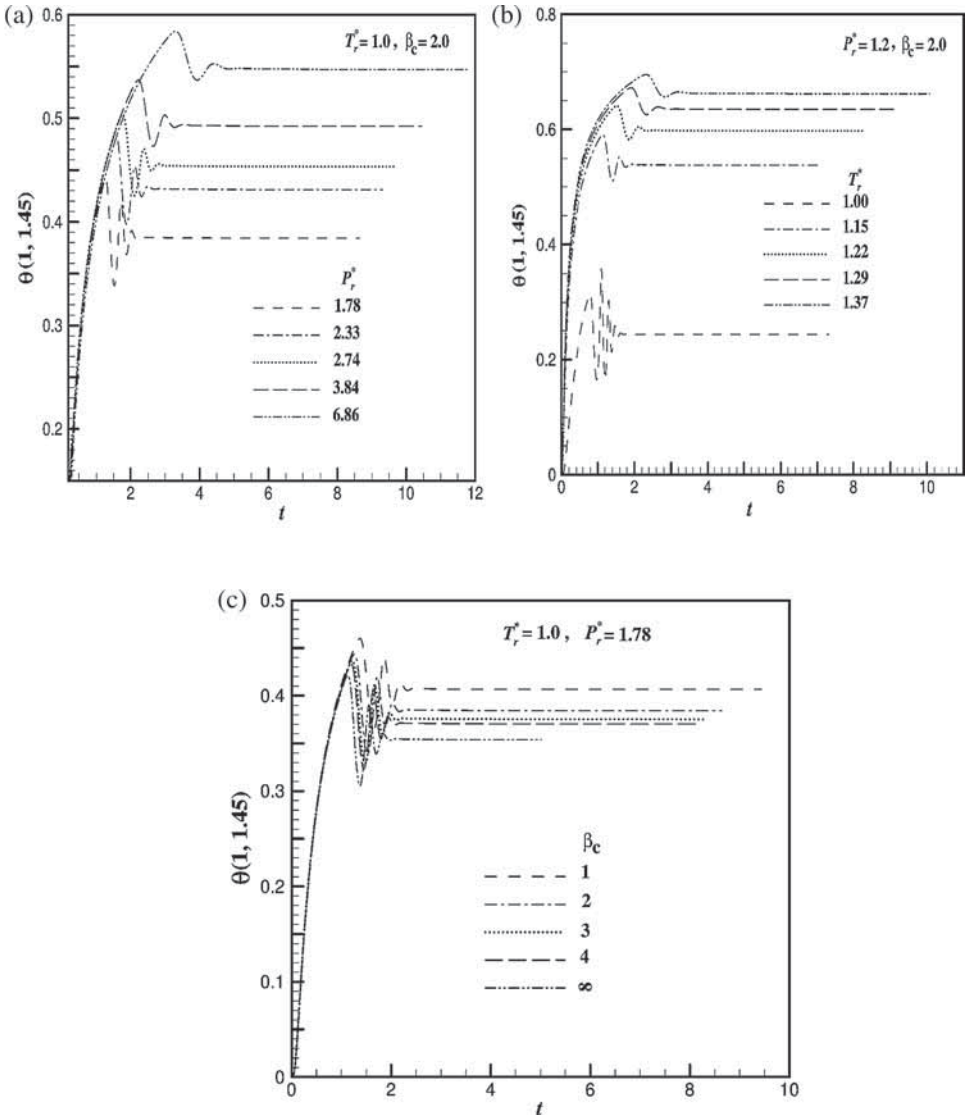


**Figure 10.** Time-dependent temperature profile ($\theta$) at (1, 1.45) against time (t) for various values of (**a**) $P_r^*$, (**b**) $T_r^*$ and (**c**) $\beta_c$.

reached. It is also perceived that the steady-state time increases for greater $P_r^*$ or $T_r^*$ values, but pertaining to $\beta_c$ value, the observation is reversed. Figure 11a reveals that increased $P_r^*$ or $T_r^*$ values yield intensification in the time-independent $\theta$ profile. This result is obviously true as increasing $P_r^*$ or $T_r^*$ leads to a decrease in Grashof (Gr) number and increase in Prandtl (Pr) number, which gives higher value of temperature. Therefore, it can be remarked that the Grashof number is more dominant than the Prandtl number on supercritical Casson fluid. From figure 11b, it can be understood that under the steady condition, the $\theta$ values increase for increased $T_r^*$. The main focus of this plot is near $T_r^* = T'/T_c = 1.0$, i.e. near a critical point, where the $\theta$ curve is observed in the proximity of the heated wall. The incentive of the above statement is the increased values of Gr and Pr, which can be found near the critical point, i.e. at the critical temperature and pressure. Hence, greater values of Gr and Pr result in the thinner boundary layer, which is followed by a decrease in the temperature. Furthermore, figure 11c illustrates that as the Casson fluid parameter increases, the temperature curve moves nearer to the hot surface.

### 5.3 *Friction and heat transport coefficients*

The heat and momentum transport coefficients are key factors in the free convective studies of heat transfer, particularly in supercritical Casson fluid. These are given as eqs (14) and (15) in the non-dimensional form:

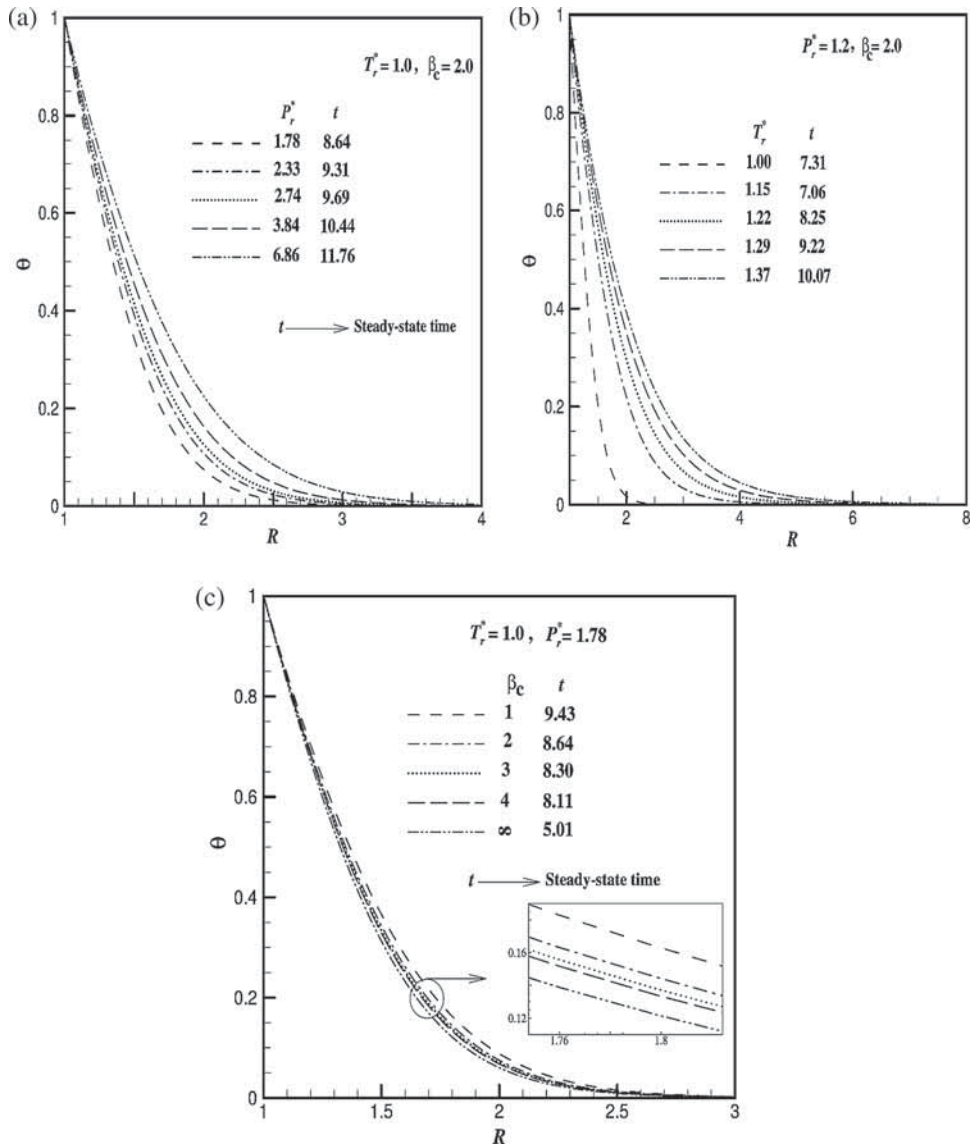


**Figure 11.** Time-independent state temperature profile ($\theta$) against $R$ when $X = 1.0$ for different values of (**a**) $P_r^*$, (**b**) $T_r^*$ and (**c**) $\beta_c$.

$$\bar{C}_f = \left(1 + \frac{1}{\beta_c}\right) \int_0^1 \left(\frac{\partial U}{\partial R}\right)_{R=1} dX, \tag{14}$$

$$\overline{Nu} = -\int_0^1 \left(\frac{\partial \theta}{\partial R}\right)_{R=1} dX, \tag{15}$$

where $\bar{C}_f$ denotes the average skin-friction coefficient and $\overline{Nu}$ indicates the average Nusselt number. In the supercritical Casson fluid region, the values of $\bar{C}_f$ against time ($t$) for different emerging parameters are presented graphically. Figures 12a– 12c reveal the influence of $P_r^*$, $T_r^*$ and $\beta_c$, respectively. The values of $\bar{C}_f$ are found to be reliable as those are comparable with velocity profiles. An inverse relation is found between the values of $\bar{C}_f$ and the values of $P_r^*$, $T_r^*$ and $\beta_c$. The reason for a decrease in $\bar{C}_f$ close to the hot surface is a decrease in the velocity values for increasing $P_r^*$ or $T_r^*$ and decreasing $\beta_c$ (refer figures 7 and 9). The key feature of figure 12b is at $T_r^* = 1.0$ (i.e. near the critical point); $\bar{C}_f$ has greater fluctuations compared to all other $T_r^*$ values. This result is obvious because near the critical point, Gr and Pr have larger values, which in turn amplify the $\bar{C}_f$ values. Furthermore, from figure 12c, it is remarked that the $\bar{C}_f$ curves are closely associated with one another in the beginning. In particular, the effect of $\beta_c$ on $\bar{C}_f$ profile is insignificant in the region $0 \leq t \leq 1$. In addition, the steady-state time decreases as $\beta_c$ increases. Again, for various values of $P_r^*$, $T_r^*$ and $\beta_c$, the $\overline{Nu}$ curves are exemplified in figures 13a–13c, respectively. These consequent

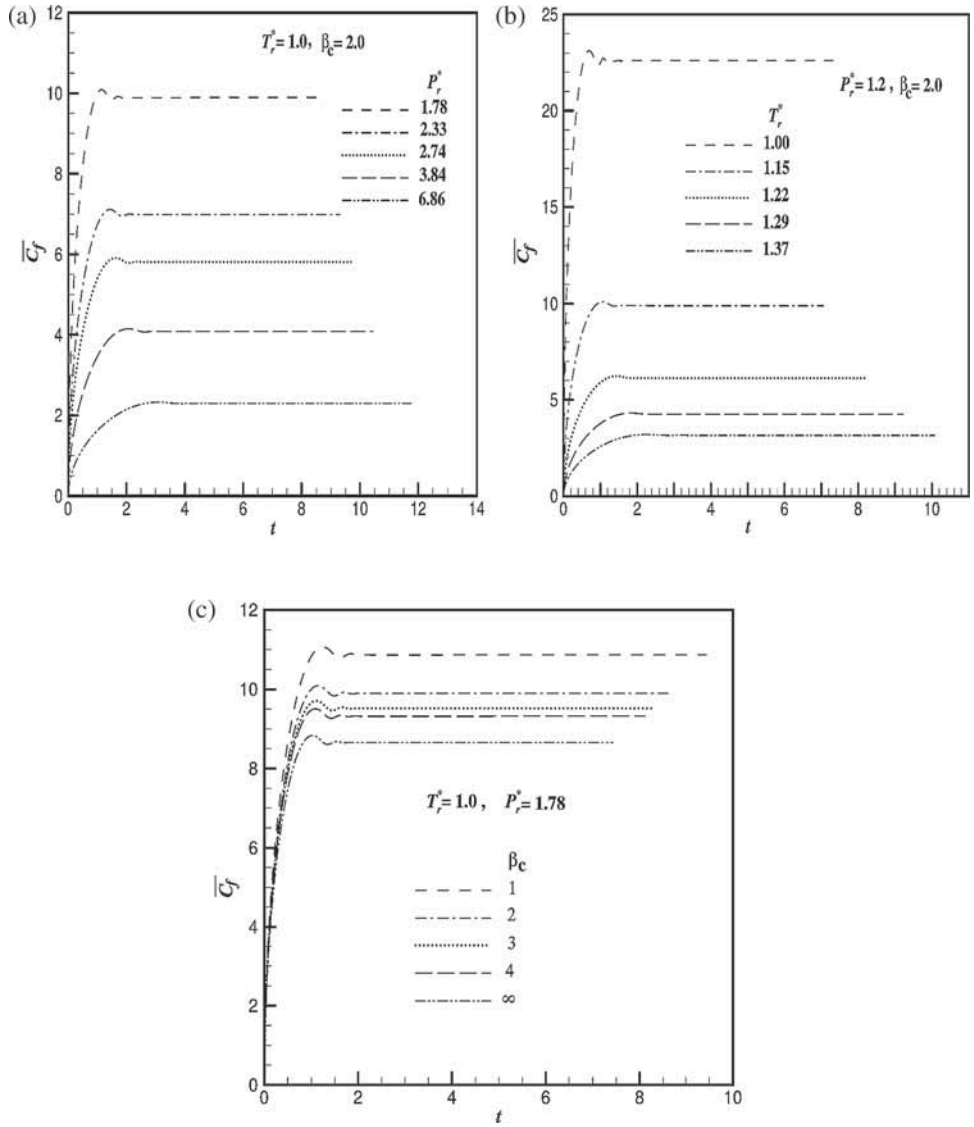


**Figure 12.** Average skin-friction coefficient ($\bar{C}_f$) for different values of (**a**) $P_r^*$, (**b**) $T_r^*$ and (**c**) $\beta_c$.

figures convey that the $\overline{Nu}$ profile decreases against time, then shows an increase and at last reaches the steady state. Also, the overlapped $\overline{Nu}$ curves reveal the fact about heat transfer due to conduction at the early time. The significant observation is that the $\overline{Nu}$ values decrease for increased values of $P_r^*$ or $T_r^*$ and for decreased values of $\beta_c$ because in the supercritical Casson fluid region, the temperature curves upsurge as $P_r^*$ or $T_r^*$ upsurges and as $\beta_c$ decreases, which yields negatively increased values of $\overline{Nu}$ [refer eq. (15) and figure 11]. Also, as the Casson fluid parameter ($\beta_c$) rises, the steady-state time decreases.

### 5.4 *Casson fluid flow variables, friction and heat transport coefficients for isobutane in three regions*

The fluids can be catagorised on the basis of critical conditions (temperature and pressure) as SCF and subcritical fluid, i.e. above and below the critical conditions, respectively (refer figure 1a).

On the basis of classification of fluids related to the critical pressure and critical temperature, the steady and unsteady flow profiles for Casson fluid, average momentum and heat transport coefficients for isobutane in the regions of subcritical, nearly critical and supercritical for different temperatures ($T'$) and pressures ($P$) are investigated and displayed in figure 14. Figure 14a presents a three-region graph for the time-dependent $U$ and $\theta$ profiles at different locations (1, 1.4) and (1, 1.45), respectively. A few important observations from figure 14a are listed here: (i) it describes the magnitude of the overshoot of $U$ and $\theta$, which is maximum at the supercritical region compared to that of the subcritical and near critical regions; (ii) the transient velocity amplifies as the pressure and temperature fluctuate from under-critical region to the supercritical region, whereas

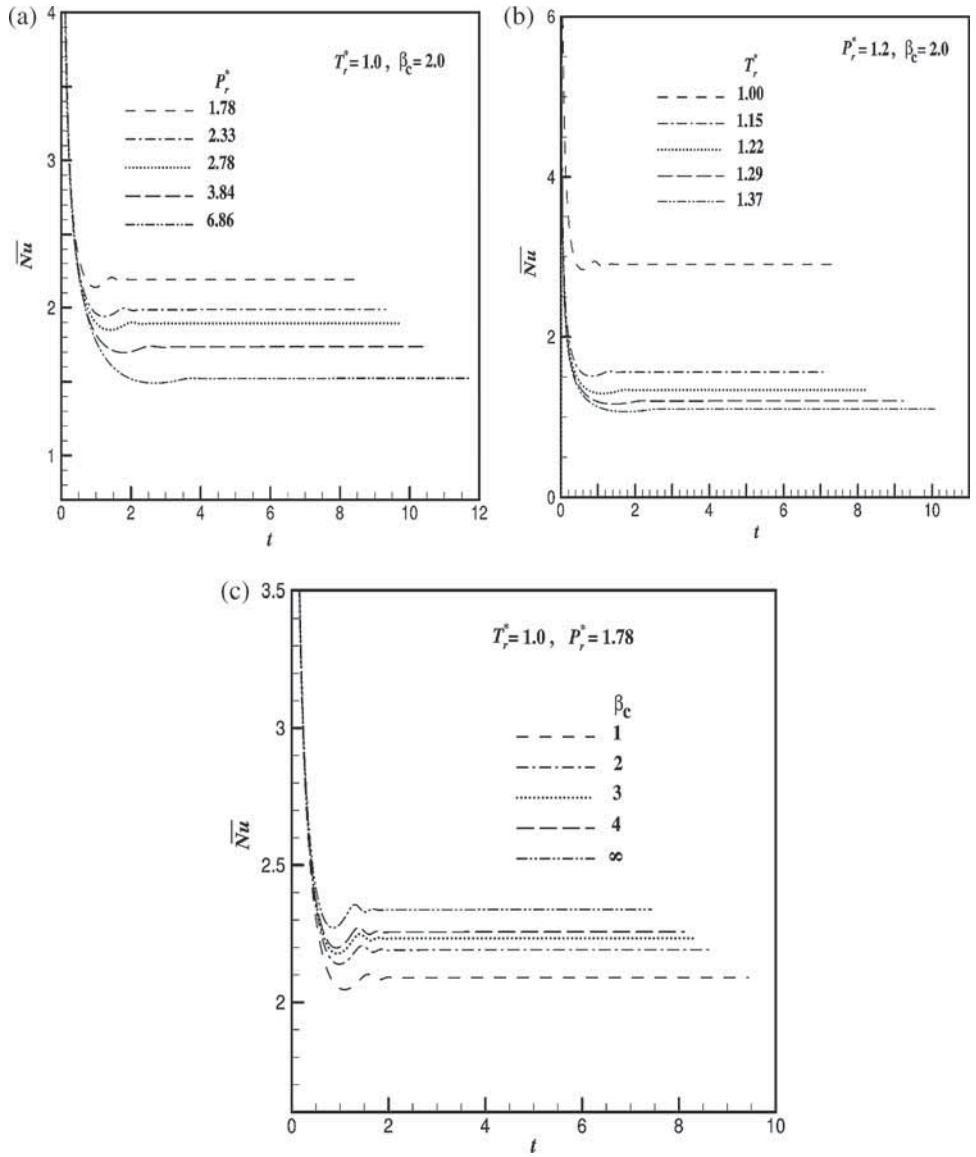


**Figure 13.** Average heat transport coefficient ($\overline{\mathrm{Nu}}$) for different values of (**a**) $P_\mathrm{r}^*$, (**b**) $T_\mathrm{r}^*$ and (**c**) $\beta_\mathrm{c}$.

for transient temperature, the opposite trend is seen; (iii) for both temperature and velocity profiles, the temporal peak time decreases as the temperature and pressure vary from subcritical region to supercritical region; (iv) owing to the phase change behaviour, sharp oscillations in transient velocity distributions are noticed; (v) these fluctuations are noticed particularly in the time period $0.5 \leq t \leq 1.5$ where oscillations decay as time progresses.

The steady-state graphs of flow variables in all regions for different pressures and temperatures against $R$ at $X = 1.0$ are displayed in figure 14b. These plots depict the results that as isobutane flows from the subcritical to the supercritical region, the velocity values increase. However, for the $\theta$ profile, it is seen to be reversed. It is also remarked that in the supercritical Casson fluid region, the momentum boundary layer is thicker, whereas the thermal boundary layer is thinner. This is true in the three regions. The steady-state time drops as the flow takes place from the subcritical to the supercritical region.

For different temperatures and pressures, figure 14c demonstrates the variation of heat transport and average momentum coefficients with time in all the regions. Here it is remarked that at the early phase of time, after $t = 0$, in all the three regions, the average heat transfer rates remain the same for all temperatures and pressures, which confirm the heat conduction. One more important observation is that there is an increment in both $\bar{C}_\mathrm{f}$ and $\overline{\mathrm{Nu}}$ as the Casson fluid flow

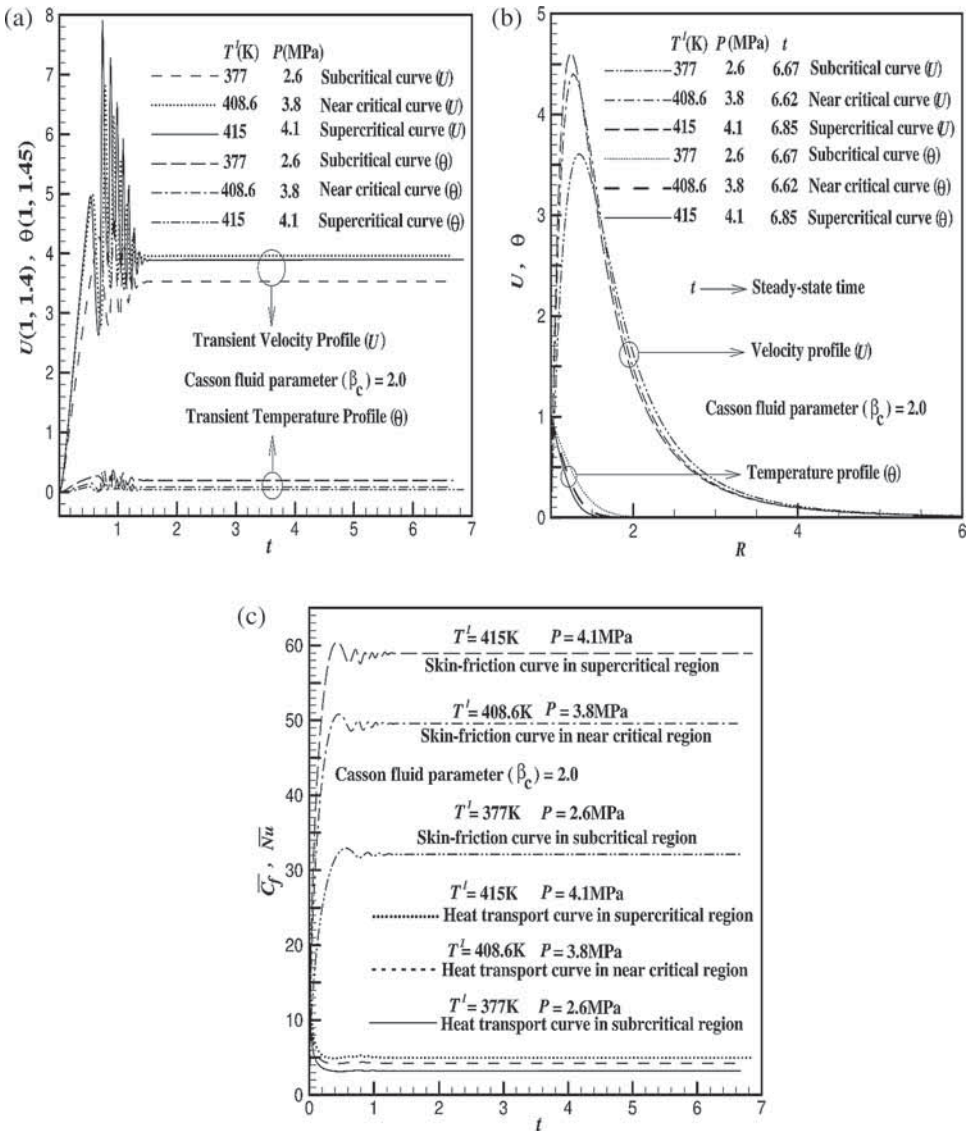


**Figure 14.** The curves in three regions for various pressures, temperatures and for fixed supercritical Casson fluid parameter, $\beta_c = 2.0$: (**a**) transient flow variables, (**b**) steady-state flow variables and (**c**) average skin-friction and heat transport coefficients.

starts from the under-critical region to the supercritical region.

## 6. Conclusions

Present numerical investigation deals with the study of supercritical heat transfer characteristics of the Casson fluid in terms of isobutane flow about an isothermal vertical cylinder using a finite difference technique in supercritical region. Furthermore, RK-EOS and VW-EOS are used to formulate the expression for the thermal expansion coefficient in the SCF region. However, the non-Newtonian Casson fluid flow model gives the nonlinear, coupled time-dependent partial differential equations and is solved using the Crank–Nicolson scheme. The following key observations were recorded based on the numerical simulations:

- A new thermodynamic model has been brought to attention using RK-EOS to visualise the free convective phenomenon in supercritical Casson fluid region.
- The calculated thermal expansion coefficient ($\beta$) values of isobutane based on RK-EOS are in close agreement with the reference values compared with VW-EOS and ideal gas assumption.
- The steady-state time for the flow profiles decreases as Casson fluid parameter $\beta_c$ increases. Furthermore,

higher values of $\beta_c$ increase the size of the overshoot of the flow velocities.
- As supercritical Casson fluid parameter ($\beta_c$) increases, the time-independent velocity increases, whereas the trend is reversed for temperature.
- The steady-state velocity profile amplifies and temperature profile decreases as the Casson fluid flow changes from the subcritical to the supercritical region.
- The average momentum transport coefficient ($\bar{C}_f$) and heat transport coefficient ($\overline{Nu}$) increase as the Casson fluid flow changes from the subcritical to the supercritical region. Also, there is a decrease in $\bar{C}_f$ and increase in $\overline{Nu}$, as $\beta_c$ increases.
- The present study can be extended to understand some of the reported literature studies such as nuclear detector instrumentation studies under low pressure [42], sinusoidal motion of Casson particle fluid [43] and Jeffrey fluid [44].

In summary, the present work can be extended to investigate the heat and mass transfer characteristics of supercritical Casson fluid in different flow configurations such as parallel disks, wedges, stretching sheets/surfaces, vertical plates, parallel plates, circular and horizontal cylinders, etc. Furthermore, the present work may be used to study the supercritical heat and mass transfer characteristics of complicated non-Newtonian fluids such as couple stress fluid, fourth-grade fluid, power-law fluid, etc.

## Acknowledgements

The first author Ashwini Hiremath wishes to thank DST-INSPIRE (Code No. IF160409) for the grant of research fellowship and the Central University of Karnataka for providing research facilities. The second author wishes to thank Maulana Azad National Fellowship program, University Grants Commission, Government of India, Ministry of Minority Affairs, MANF (F1-17.1/2017-18/MANF-2017-18-KAR-81943) for the grant of research fellowship and the Central University of Karnataka for providing research facilities. Furthermore, the authors wish to express their gratitude to the reviewers who highlighted important areas for improvement in this paper. Their suggestions have served specifically to enhance the clarity and depth of the interpretation in the paper.

## References

[1] E M Sparrow and J L Gregg, *Trans. ASME* **78**, 18 (1956)
[2] H R Lee, T S Chen and B F Armaly, *J. Heat Transfer* **110**, 103 (1988)
[3] A Shariati and C J Peters, *Curr. Opin. Solid State Mater. Sci.* **7**, 371 (2003)
[4] Y Jaluria, *Natural convection heat and mass transfer* (Pergamon Press, Oxford, 1980)
[5] M A McHugh and V J Krukonis, *Supercritical fluid extraction, principles and practice*, 2nd edn (Butterworth-Heinemann, Boston, 1994)
[6] A Rolando, *Natural convection heat transfer in supercritical fluids*, M.Sc. thesis (Mechanical Engineering, University of Puerto Rico, USA, 2004)
[7] A R Teymourtash, D R Khonakdar and M R Raveshi, *J. Supercrit. Fluids* **74**, 115 (2013)
[8] S Pandey, E Laurien and Xu Chu, *Int. J. Therm. Sci.* **117**, 227 (2017)
[9] D R Khonakdar and M R Raveshi, *J. Supercrit. Fluids* **107**, 549 (2016)
[10] E Kiran, P G Debenedetti and C J Peters, Supercritical fluids: fundamental and applications, in *NATO science series* (Springer, USA, 2000)
[11] M K S Sarkar and D N Basu, *Int. J. Therm. Sci.* **111**, 30 (2017)
[12] B Shen and P Zhang, *Int. J. Therm. Sci.* **71**, 1 (2013)
[13] Y Cao and X-R Zhang, *Int. J. Therm. Sci.* **58**, 52 (2012)
[14] E A Muller and L A Estevez, *J. Supercrit. Fluids* **3**, 136 (1990)
[15] B Shen and P Zhang, *Int. J. Therm. Sci.* **89**, 136 (2015)
[16] G Janardhana Reddy, H Basha and N S V Narayanan, *J. Mol. Liq.* **250**, 131 (2018)
[17] G Janardhana Reddy, H Basha and N S V Narayanan, *J. Mol. Liq.* **259**, 209 (2018)
[18] D N Thompson, D M Ginosar and K C Burch, *Appl. Catal. A: Gen.* **279**, 109 (2005)
[19] A K Suresh, *J. Supercrit. Fluids* **12**, 165 (1998)
[20] R R Shiriyazdanov, *Russ. J. Phys. Chem. B* **5(7)**, 1080 (2011)
[21] J Sarkar and S Bhattacharyya, *Int. J. Therm. Sci.* **48**, 1460 (2009)
[22] M Nishikawa, Y Yamaguchi and K Fujita, *J. Chem. Phys.* **61(6)**, 2356 (1974)
[23] N M Sanchez, O S G P Soares, M F R Pereira, M Jesus Sanchez-Montero, J L Figueiredo and F Salvador, *Appl. Catal. A: Gen.* **502**, 71 (2015)
[24] A E Koklin, V M Kh Chan and V I Bogdan, *Russ. J. Phys. Chem. B* **8(8)**, 991 (2014)
[25] A E Koklin, V M Kh Chan, V B Kazanskii and V I Bogdan, *Kinet. Catal.* **51(3)**, 410 (2010)
[26] S Herrmann, E Hassel and E Vogel, *AIChE J.* **61(9)**, 3116 (2015)
[27] G Funamoto, S Tamura, K Segawa, K T Wan and M E Davis, *Res. Chem. Intermed.* **24(4)**, 449 (1998)
[28] G Makanda, S Shaw and P Sibanda, *Bound. Value Probl.* **2015**, 2 (2015)
[29] C S K Raju, N Sandeep, V Sugunamma, M Jayachandra Babu and J V Ramana Reddy, *Eng. Sci. Technol. Int. J.* **19**, 45 (2016)

[30] M Mustafa, T Hayat, I Pop and A Aziz, *Heat Transfer Asian Res.* **40**, 563 (2011)
[31] M Y Malik, M Naseer, S Nadeem and A Rehman, *Appl. Nanosci.* **4**, 869 (2014)
[32] G Janardhana Reddy, B Kethireddy, J C Umavathi and M A Sheremet, *Therm. Sci. Eng. Prog.* **5**, 172 (2018)
[33] G Janardhana Reddy, B Kethireddy, M Kumar and M M Hoque, *J. Mol. Liq.* **252**, 245 (2018)
[34] G Soave, *Fluid Phase Equilib.* **82**, 345 (1993)
[35] S J Blundell and K M Blundell, *Concepts in thermal physics* (Oxford University Press, UK, 2006)
[36] N Casson, *Rheology of disperse systems* edited by C C Mill (Pergamon Press, Oxford, 1959) pp. 84–102
[37] A K A Hakeem, P Renuka, N V Ganesh, R Kalaivanan and B Ganga, *J. Magn. Magn. Mater.* **401**, 354 (2016)
[38] H P Rani, G J Reddy and C N Kim, *Appl. Math. Mech.* (English edition) **34(8)**, 985 (2013)
[39] B E Poling, J M Prausnitz and J P O'Connell, *The properties of gases and liquids*, 5th edn (McGraw-Hill, New York, 2001)
[40] R D Goodwin and W M Haynes, *Thermophysical properties of isobutane from 114 to 700 K at pressures to 70 MPa* (U.S. Department of Commerce, 1982)
[41] A J Ede, *Advances in free convection* (National Engineering Laboratory, East Kilbride Scotland, 1967)
[42] A Jhingan, *Pramana – J. Phys.* **85(3)**, 483 (2015)
[43] M M Bhatti, A Zeeshan and R Ellahi, *Pramana – J. Phys.* **89(3)**: 3 (2017)
[44] M Kumar, G J Reddy and N Dalir, *Pramana – J. Phys.* **91(5)**: 1 (2018)